ADVENTURES in ASTROPHYSICAL X-RAY SPECTROSCOPY

We're facing a Golden Age in X-ray astronomy!

- sub-arcsec broadband spectroscopic imaging
- opening up spectroscopy:
  grating spectrometers on AXAF, XMM,
  microcalorimeter on Astro-E

Spectroscopy:

- Vastly increased sensitivity ($\lambda/\Delta\lambda$, A_{eff})

  ⇨ Approach lab standards;
  full array of traditional laboratory spectroscopic techniques becomes accessible, and <u>move</u>:

  - very low n
  - very high T
  - large optical depth
  - strong radiation fields
  - ⋮

Columbia, Nov 3 '99

- Most emphasis to date on 'traditional', collisionally dominated plasma's (coronae, SNR, clusters, hot gas in ISM's, ...)
- lots of experience from terrestrial experiments carries over (fusion plasma's, etc.). Also: solar coronal spectroscopy.
- in this talk, focus on some unexpected stuff — less predictable & more fun
- three topics:
  1) spectroscopy of interstellar dust grains
  2) spectroscopy of X-ray photoionized gas, w/ application to GRB's
  3) direct X-ray spectroscopic distances to clusters, & the size of the Universe

1. EXAFS Spectroscopy of Interstellar (and extragalactic ?) Dust

EXAFS: "Extended X-ray Absorption Fine Structure"

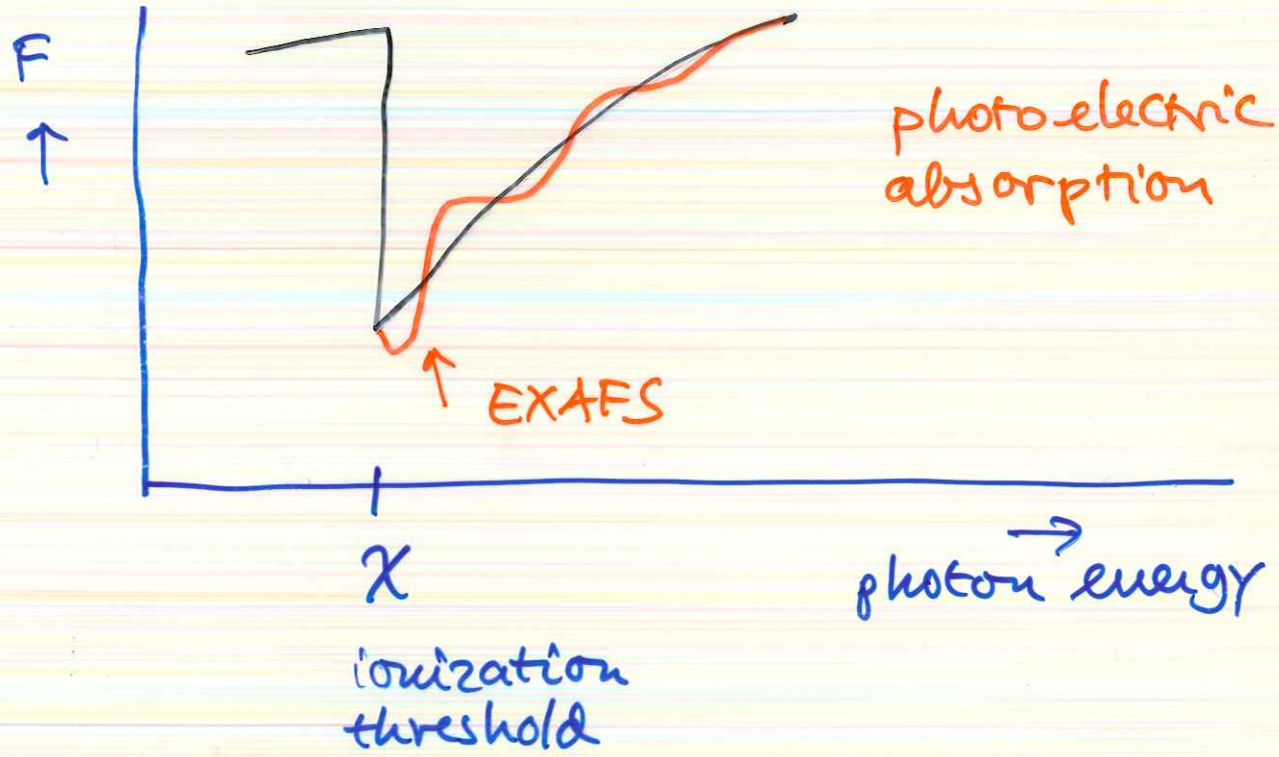

- Quantum interference effect in photoelectric absorption transition probability
- in atoms embedded in material with short-range order:

  solids, molecules

  ↓

  dust!

mechanism:

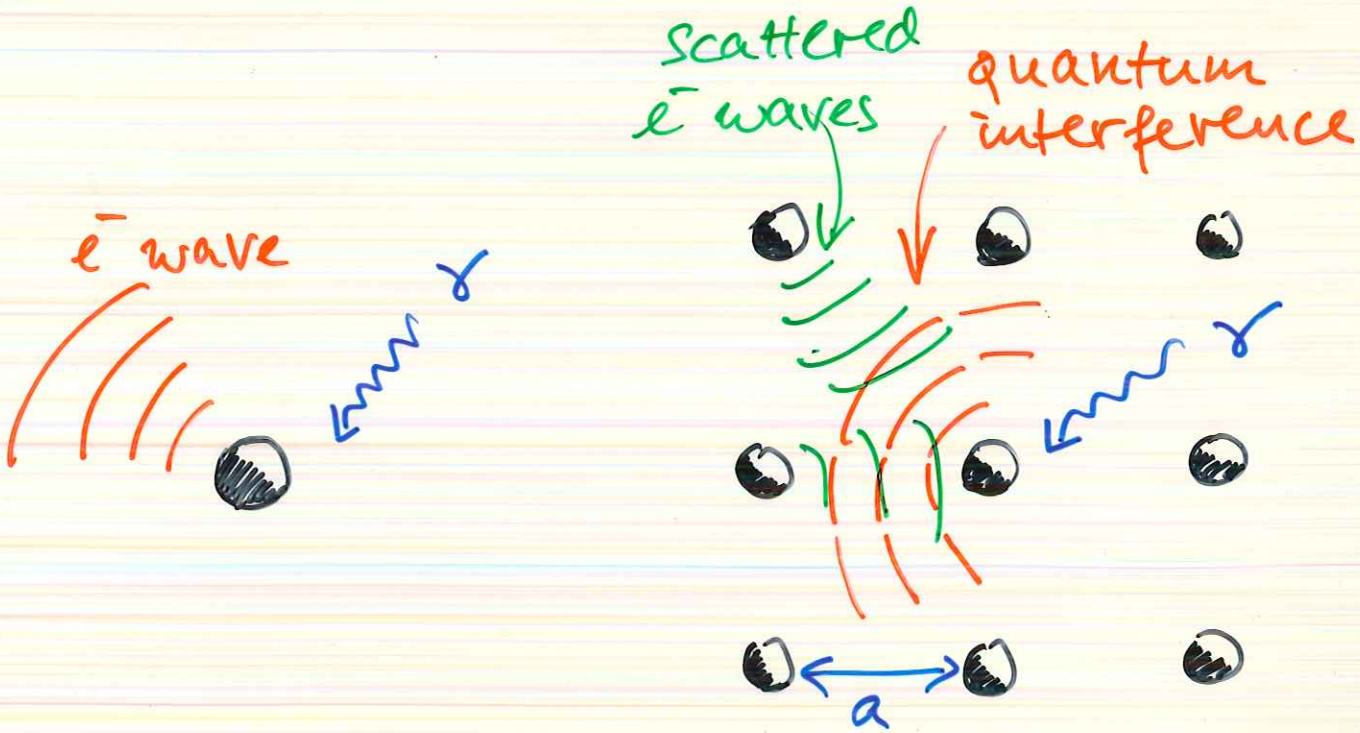

free atom

short-range order

- transition probability:

$$\left| \langle f + f_{scatt} | H_{int} | i \rangle \right|^2$$

↑ modulation!

- resonances at $2ka \sim 2n\pi$
  ($k = p/\hbar$ of the photoelectron)

$$\frac{\hbar^2 k^2}{2m_e} = E_\gamma - \chi \Rightarrow E_n \sim \chi + \frac{h^2}{8m_e a^2} \cdot n^2$$

$$\Rightarrow \Delta E_\gamma \sim \frac{h^2}{8m_e a^2}$$

$$\sim 38 \left(a/1\text{Å}\right)^{-2} \text{ eV}$$

Not a joke!

EXAFS in beam filters on EXOSAT (1983)

Al L-edge (171 Å)

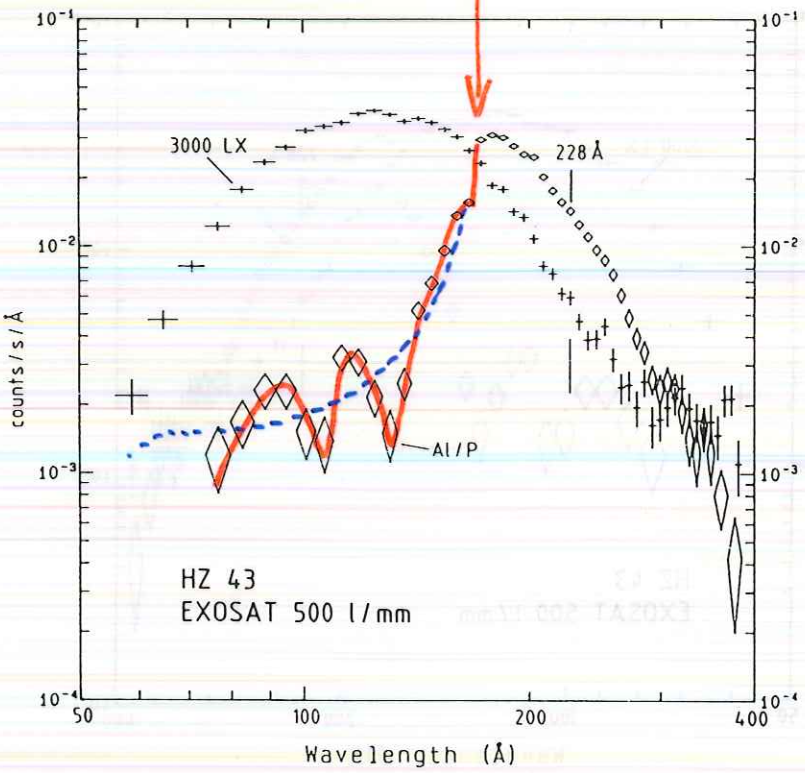

FIG. 2.—Measured countrate spectra of HZ 43 with the 500 lines mm^{-1} spectrometer, with the 3000LX filter (*crosses*) and with the Al/P filter (*diamonds*). Left and right orders are summed, and a constant background is subtracted. Error bars indicate errors derived from photon counting statistics only. Location of the He II Lyman edge at 228 Å is indicated.

HZ43: hot ($T_{eff} \sim 50{,}000$K) DA white dwarf; bright EUV/soft X-source

- Modulation in Al filter absorption curve quantitatively consistent with EXAFS in Al.
- concern for instrument calibration; but only visible with resolution > CCD!

SiO_2 (at O K)

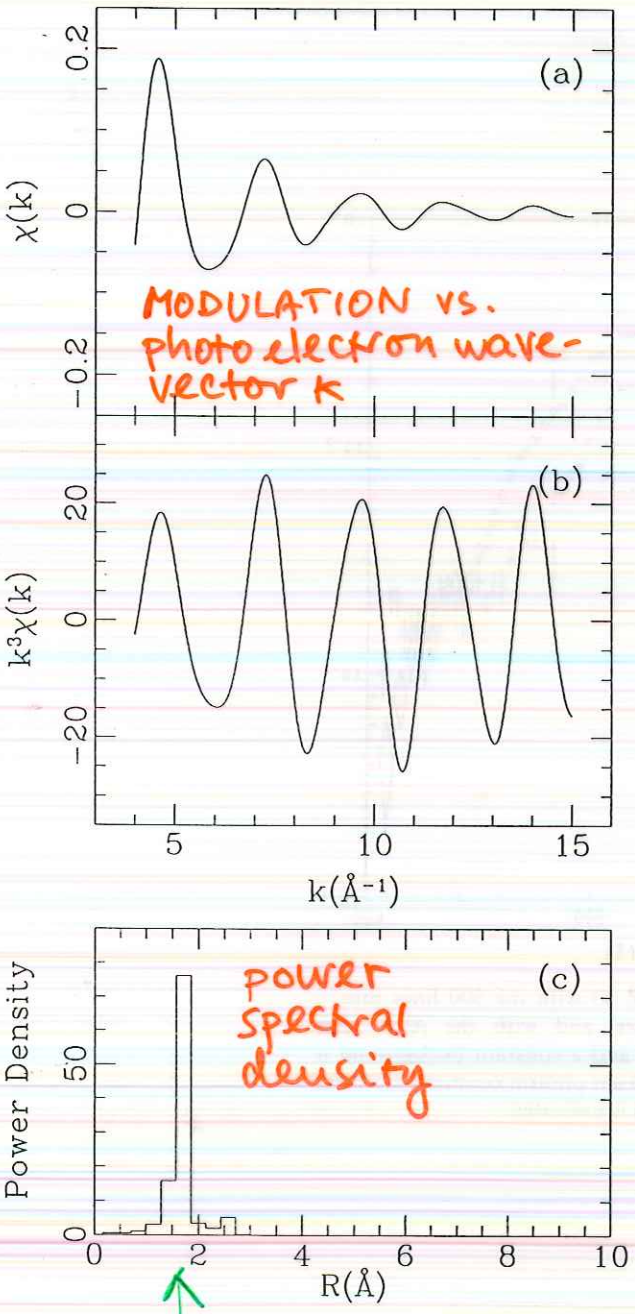

FIG. 2.—Predicted O K-edge EXAFS of SiO_2 from the AEA tool: (*a*) $\chi(k)$; (*b*) $k^3\chi(k)$; (*c*) power density spectrum of (*b*).

lattice spacing!

$MgSiO_3$ (at Mg K)

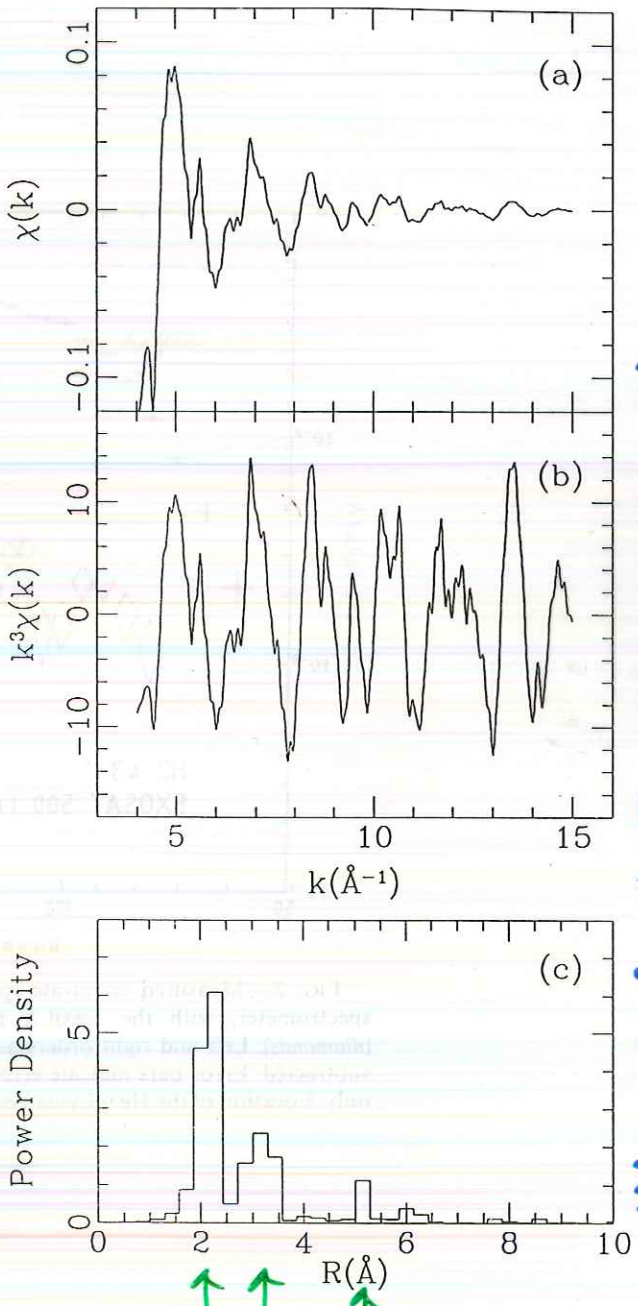

FIG. 3.—Predicted Mg K-edge EXAFS of $MgSiO_3$ from the AEA tool: (*a*) $\chi(k)$; (*b*) $k^3\chi(k)$; (*c*) power density spectrum of (*b*).

more complex lattice

Woo et al., ApJ, 477, 235 (1997)

Obvious application: X-ray absorption by interstellar dust! (major fractions of O, Si, Mg, Fe, ... in dust)

AXAF AO1 : Crab

$n_H \approx 3.10^{21}\,cm^{-2} \rightarrow \tau(0K) = 1$!

7

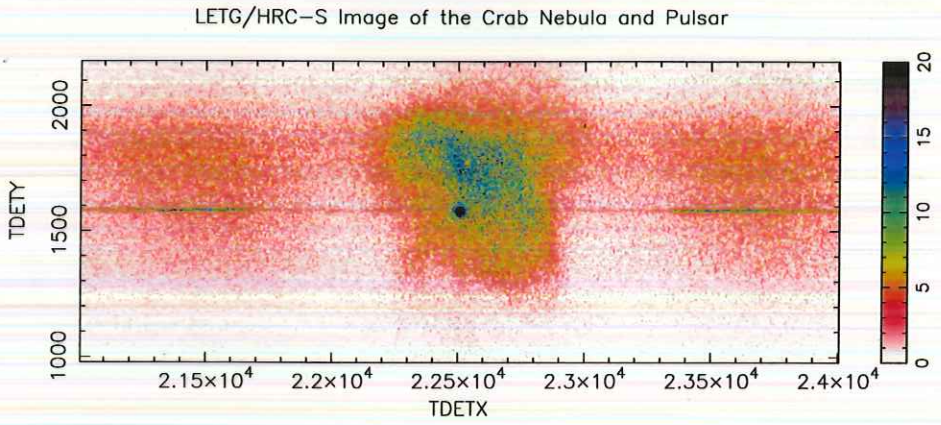

Figure 3: Simulated LETG/HRC-S image of the Crab Nebula and time-averaged Pulsar. The input is the synthesis of the pulse-off ROSAT image and the time-averaged point-source Pulsar (highly saturated in this image) convolved with the AXAF point spread function, blurred to account for aspect errors.

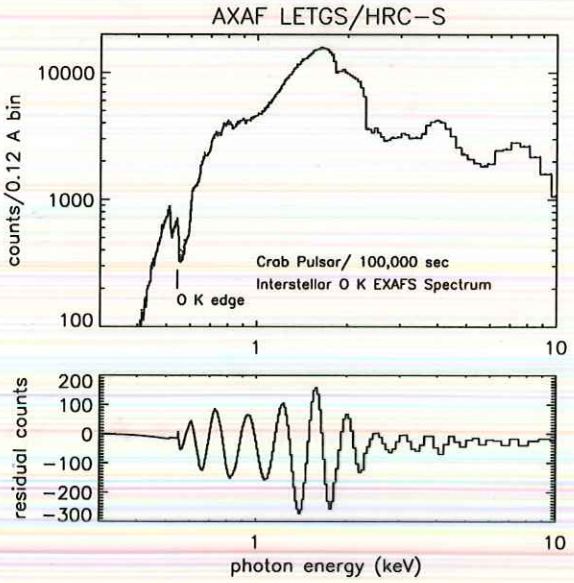

Figure 4: Simulation of an LETG/HRC-S spectrum of the Crab Pulsar, showing EXAFS from solid-state oxygen in the ISM. The lower panel shows residuals to a fit to the spectrum for gas-phase absorption only.

Due to its amplitude and its extended wave-like pattern, the simulated modulation is detectable at high statistical significance. However, systematic effects complicate the analysis and demand careful review of the calibration accuracy. We believe that we have the relevant experience to extract the EXAFS modulation from the data and thus gain some insight into the oxygen content of interstellar dust grains.

3.4 Spectroscopy of the Nebula

Deconvolving spectral from spatial information in dispersed spectra of extended objects is difficult. For the LETG, higher order contributions and dispersion by the gratings' fine support structure further complicate the analysis. Nonetheless, we believe that such an analysis is potentially useful. The degree of success in this deconvolution depends somewhat on the range of roll angles over which spectra are acquired. However, because this is not a primary objective of our observations, we shall impose no roll constraint.

References

Aschenbach, B., & Brinkmann, W. 1975, An. & Ap., 41, 147.

Blair, W. P., et al. 1997, Ap. J., 109, 473.

Brinkmann, W., et al. 1985, Nature, 313, 662.

Evans, A. 1986, M.N.R.A.S., 223, 219.

Hester, J. J., et al. 1995, Ap. J., 448, 240.

Kraft, R. P., et al. 1997, unpublished SPIE presentation, `http://hea-www.harvard.edu/HRC/`.

Paerels, F. B. S., et al. 1986, Ap. J., 308, 190.

Schattenburg, M. L., & Canizares, C. R. 1986, Ap. J., 301, 759.

Tsuruta, S. 1997, Phys. Reports, 292, 1.

Umeda, H., et al. 1993, Ap. J. Suppl., 74, 449.

Woo, J. W. 1995, Ap. J., 447, L129.

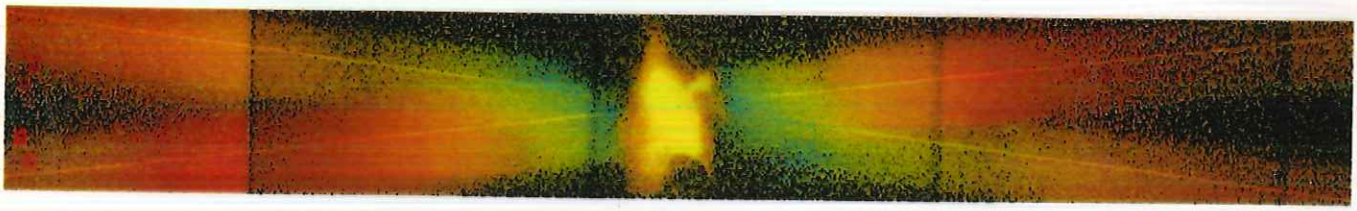

OBS ID 168 : HETGS/ACIS : Crab

2700 sec exposure, 370 counts s^{-1}

⇨ t-resolution insufficient to gate on point source (lose factor ~ 10 in sensitivity!)

DISCRETE EMISSION FROM X-RAY PHOTOIONIZED GAS, with an application to GRB 970508

Very distinctive spectral diagnostic for photoionization:

photoionized gas

COOL ($kT_e \ll \chi$)

(solve coupled eq.'s ionization, thermal eq. → $kT_e \ll \chi$; cf. H II regions!)

collisionally ionized gas:

HOT ($kT_e \sim \chi$)

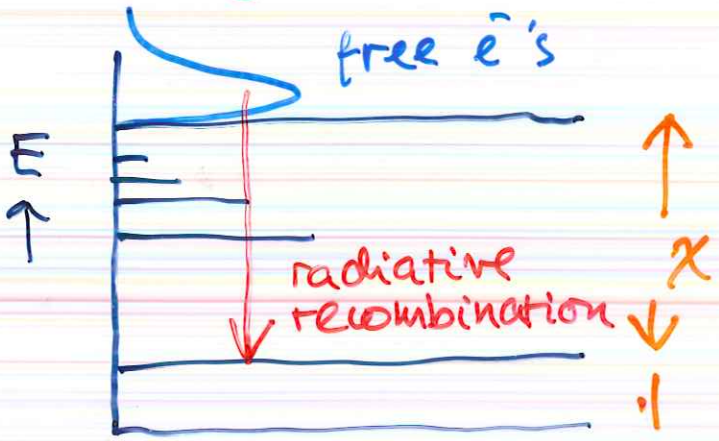

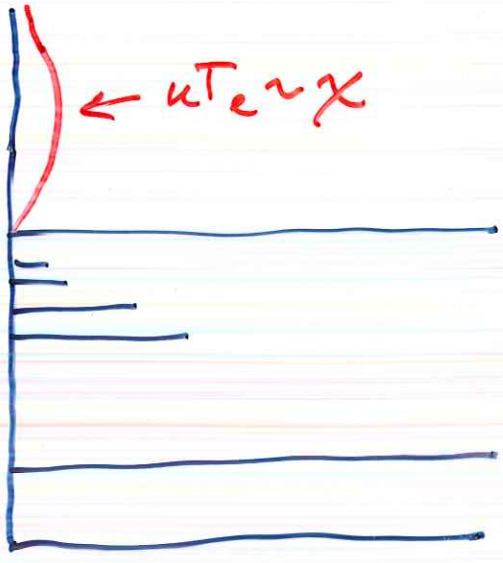

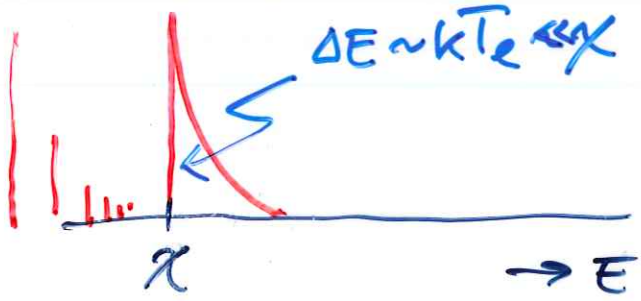

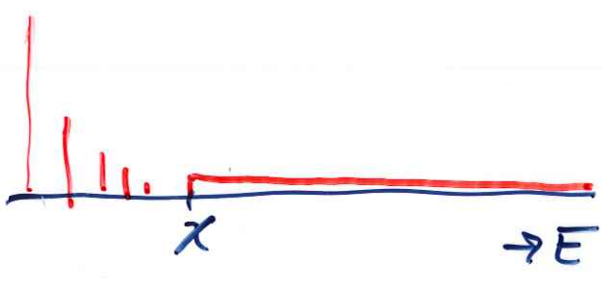

X-RAY PHOTOIONIZED GAS : CYG X-3

tenuous wind from WR companion star

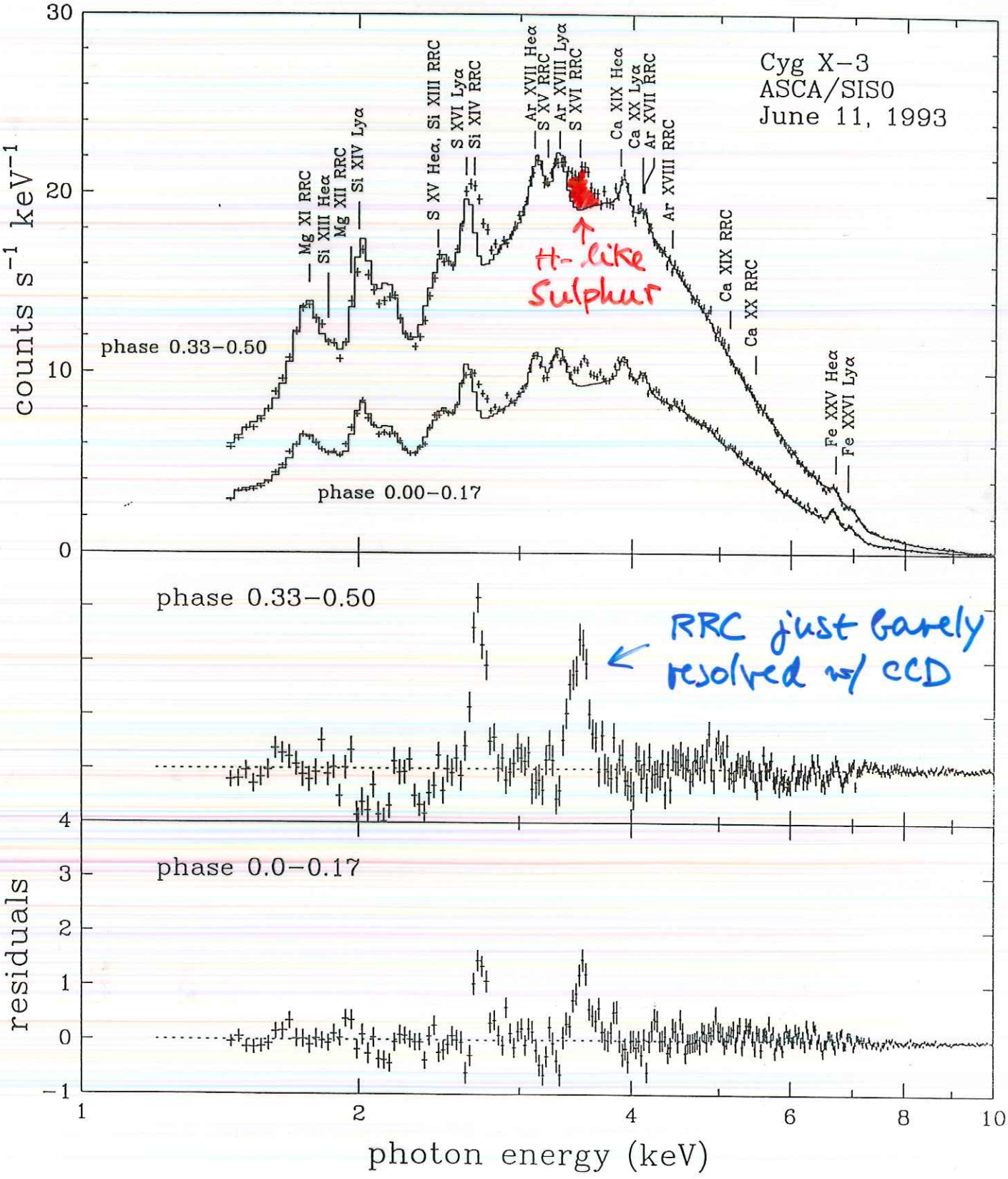

1) narrow RRC : unique signature
2) width direct measure of kT_e

Chandra HETG GTO observation: Oct. 20 '99

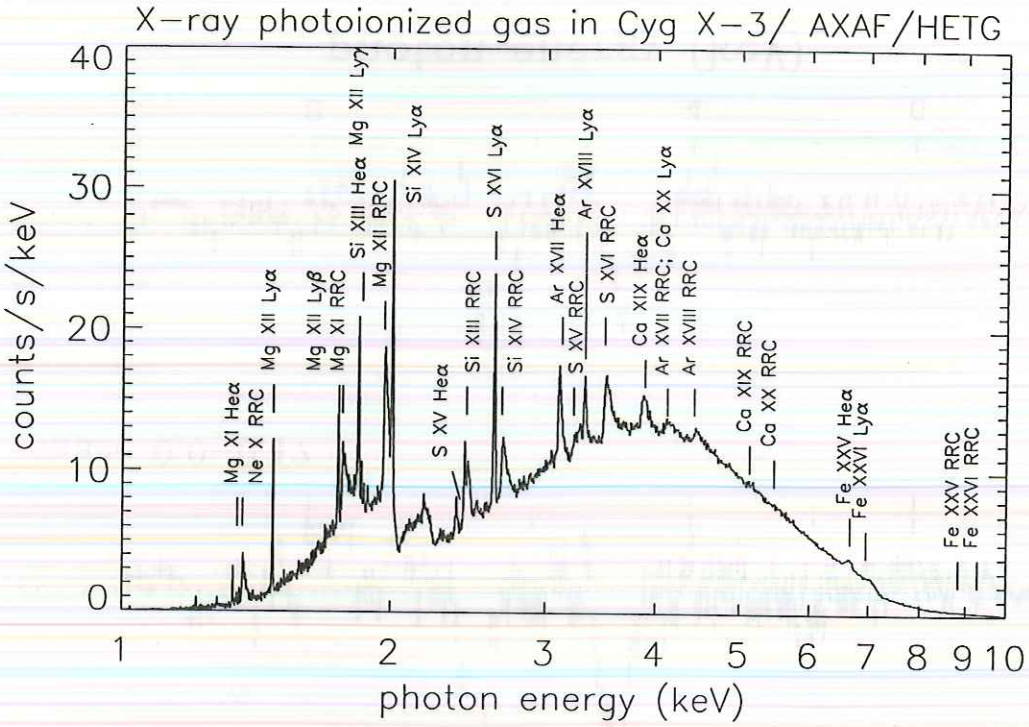

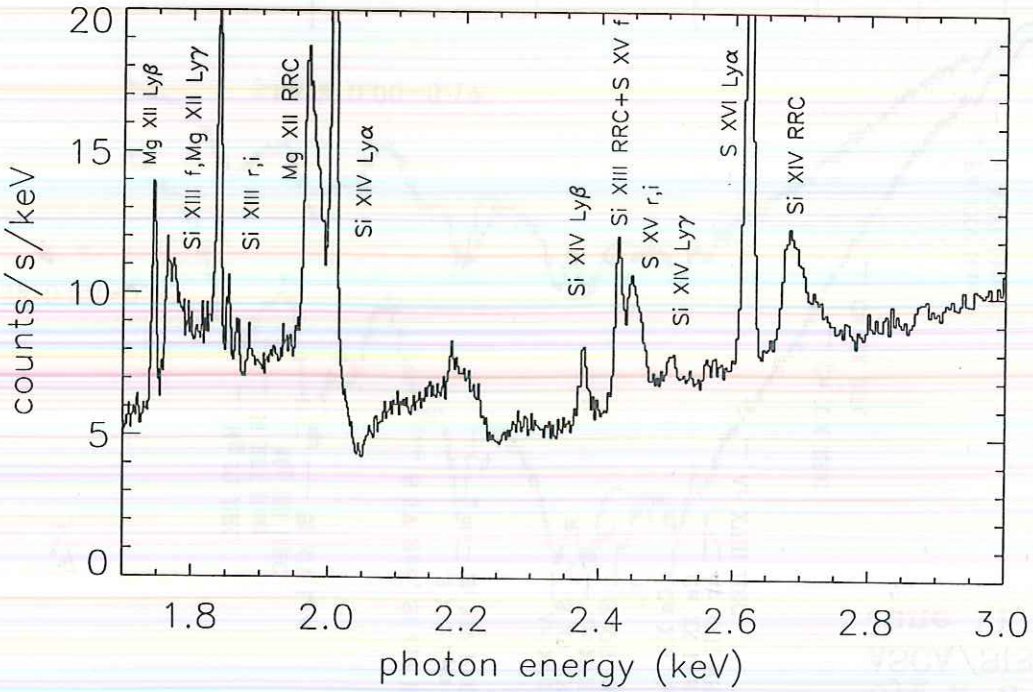

Application to GRB Afterglow X-ray Spectra?

GRB 970508, approx. 1 day into decay; BeppoSAX MECS data

just before "reburst"

during "reburst"

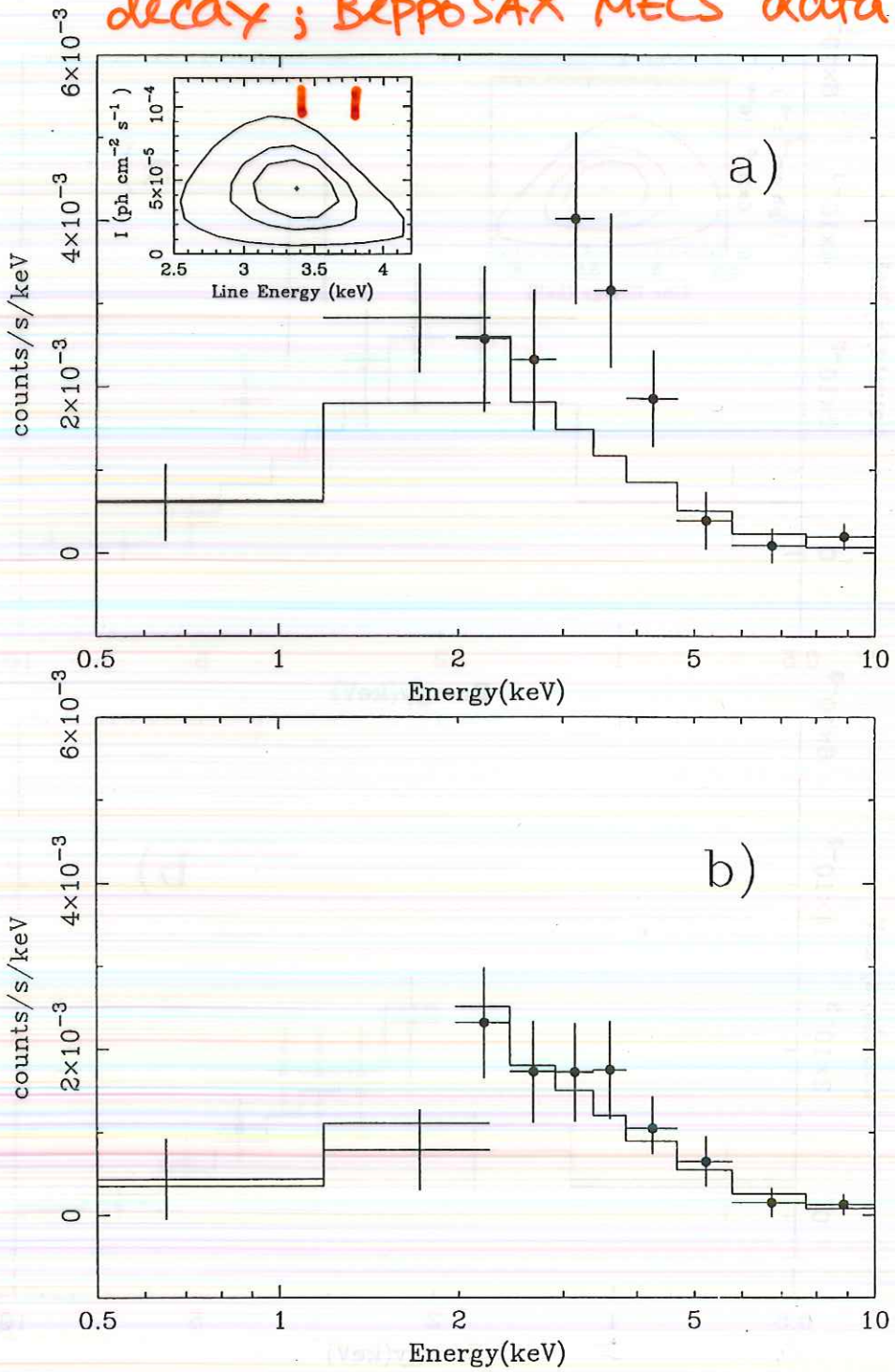

Pian & al., 1999, ApJ Letters, 519, L73

FIG. 2.—Spectra (in detector counts) of the afterglow of GRB 970508 from (*a*) data set 1a and (*b*) data set 1b. The continuous line represents the best-fit power-law continuum in the range 0.1–10 keV, excluding the interval 3–4 keV. For clarity, we show in figure LECS data below 2 keV and MECS data above 2 keV. The inset in panel *a* shows the contour plot of the line intensity vs. energy. Contours correspond to 68%, 90%, and 99% confidence levels for two interesting parameters.

$z_{optical} = 0.835$ (Metzger & al.): fits measured centroid, Fe I-XXVI

- Emission feature could be :

  1) a statistical fluctuation

  2) real ; if real :

     * emission by fluorescence
     * " " recombination
     * " " collisional excitation

- Each of these implies very different total mass of Fe (RR > fl > CX)

- RR can already be excluded : should show narrow RRC in addition to n=2-1

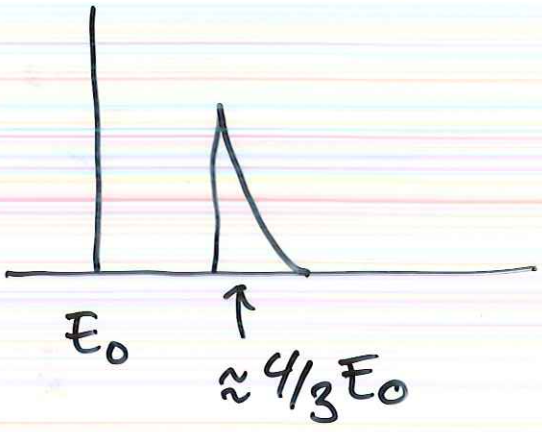

  - either z_{fit} does not match $z_{optical}$, or
  - need to suppress RRC by assuming $T > 10^8$ K

- Hardly conclusive stuff ; but : AXAF, XMM, Astro-E afterglow spectroscopy may show interesting stuff! (e.g. X-ray redshifts, ...)

3. Radiative Transfer Effects in cluster Fe Spectra; & "the size of the Universe."

- Intracluster Medium in the Great Clusters hot ($kT \sim 10$ keV), extremely luminous ➡ physical state of ICM best probed with Fe spectroscopy

  (T, n, abundances, stratification, relaxation, maybe v-fields...)

- subtle effect: clusters may be <u>optically thick</u> in strong lines:

$$\tau(\nu_0) \cong 3 \left(\frac{n_0}{10^{-3}\,cm^{-3}}\right)\left(\frac{r_c}{250\,kpc}\right)\left(\frac{A}{A_\odot}\right) f \left(\frac{10^7 K}{T_e}\right)^{\frac{1}{2}}$$

$\approx \frac{1}{3}$ ↑ ↑ 0.7 He-like Fe

- resonance scattering redistributes intensity on the sky; does not change photon nr. (and no photon destruction mechanisms in ICM).

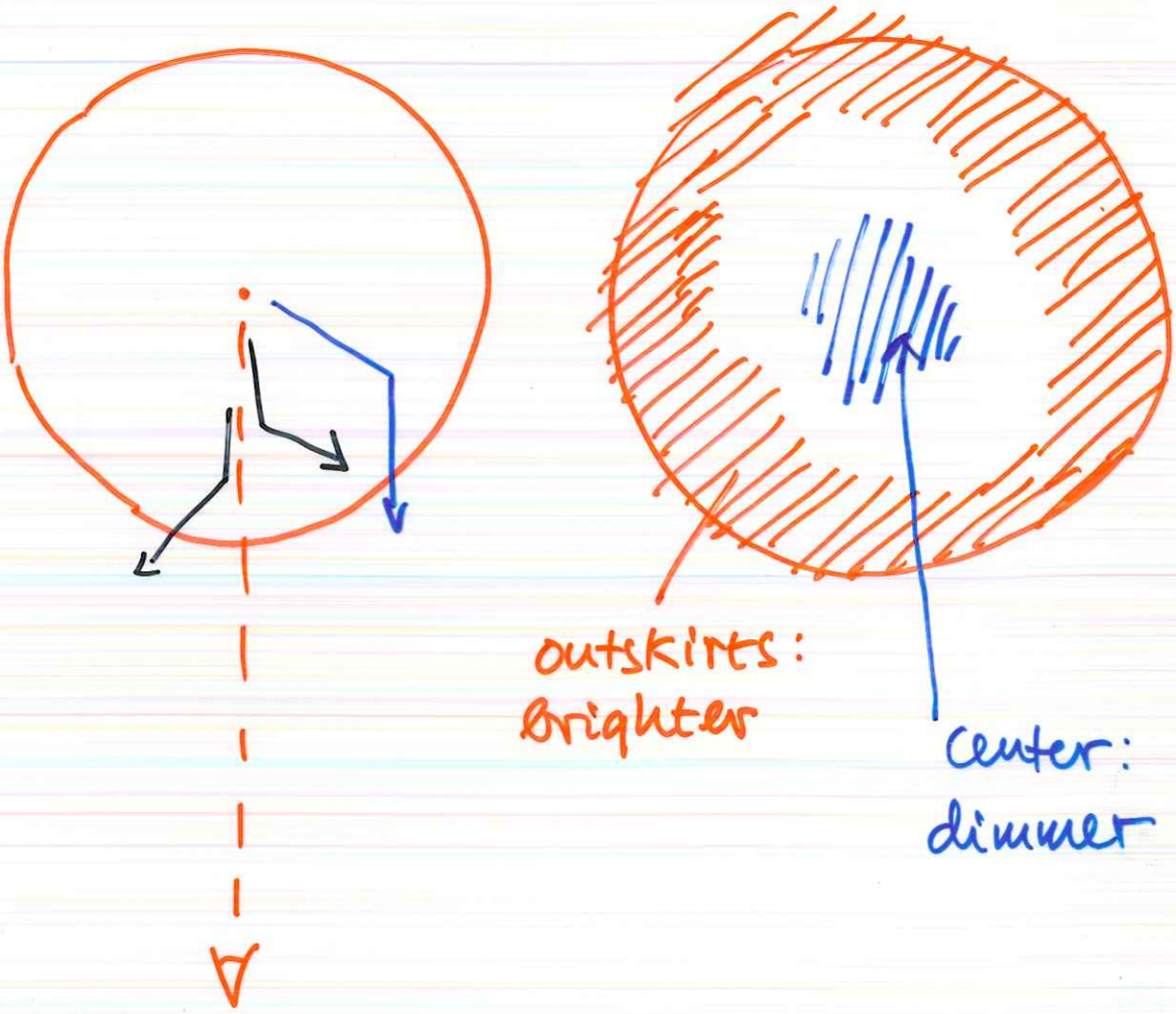

→ obvious implications for interpretation of temperature &/or abundance ∇'s.

→ first suggested by Gil'fanov, Sunyaev & Churazov (1987).

→ will also allow you to measure absolute size of the cluster!! (analogous to SZ effect)

courtesy John Peterson

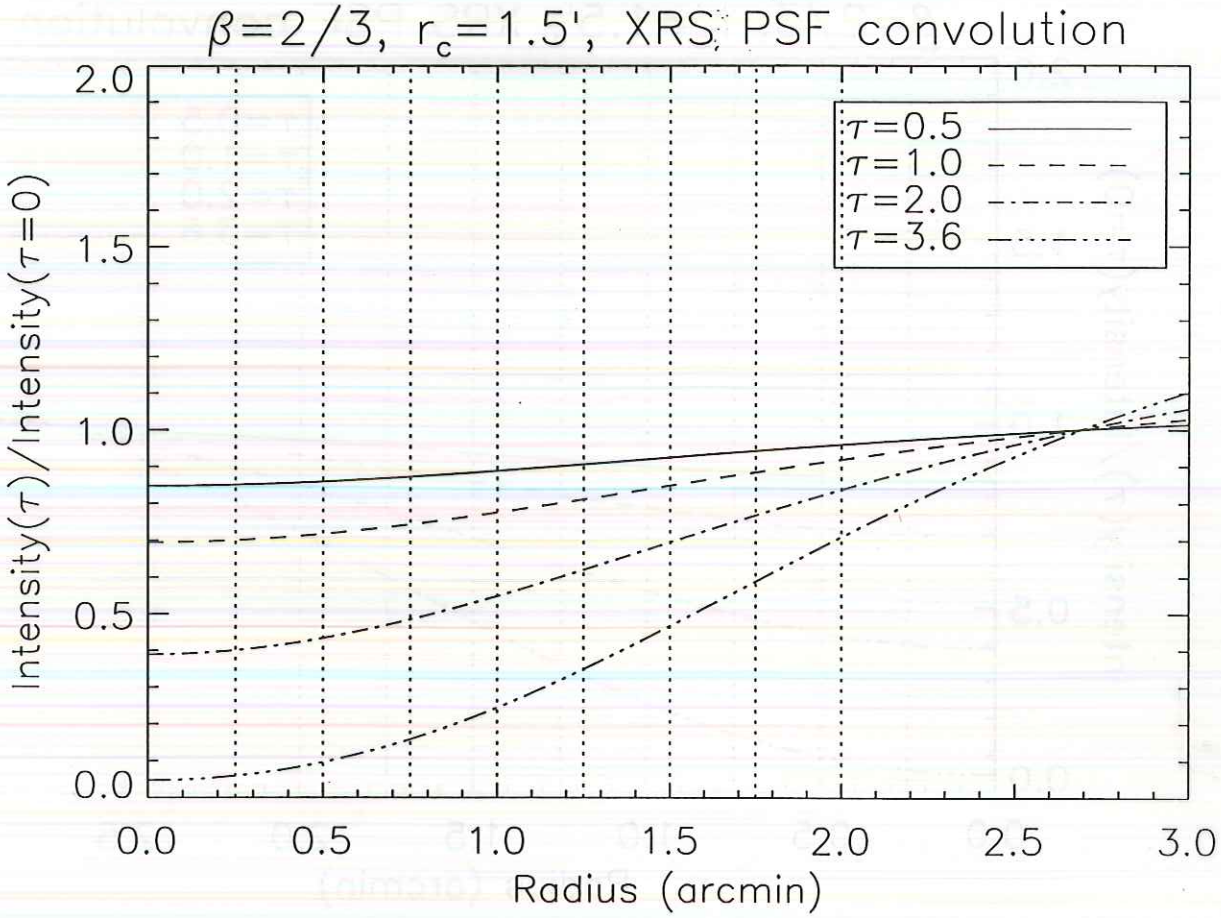

- total line flux $\propto \frac{n^2 R^3}{D^2}$
- resonance scattering depth $\propto nR$
- angular size $\theta = R/D$

3 constraints on three unknowns

$\Rightarrow$ R, D in cm, n in cm^{-3}!

and, with $V_{rad} \rightarrow H_0$! from the spatially resolved X-ray spectrum only.

Ideal experiment:

- Two monochromatic emission-line maps, one line $\tau > 0$, one line $\tau \to 0$
- same ion (no ionization balance)
- intrinsically weak T-dependence $\frac{\text{line 1}}{\text{line 2}}$

➡ good candidate:
resonant, forbidden $n = 2-1$ He-like Fe

- He-like Fe abundant broad range kT_e
- resonance line $\tau \gtrsim 1$,
  forbidden $\tau = 0$

➡ Need fairly high spectral resolving power
($\Delta E \lesssim 10$ eV or $R > 700$)

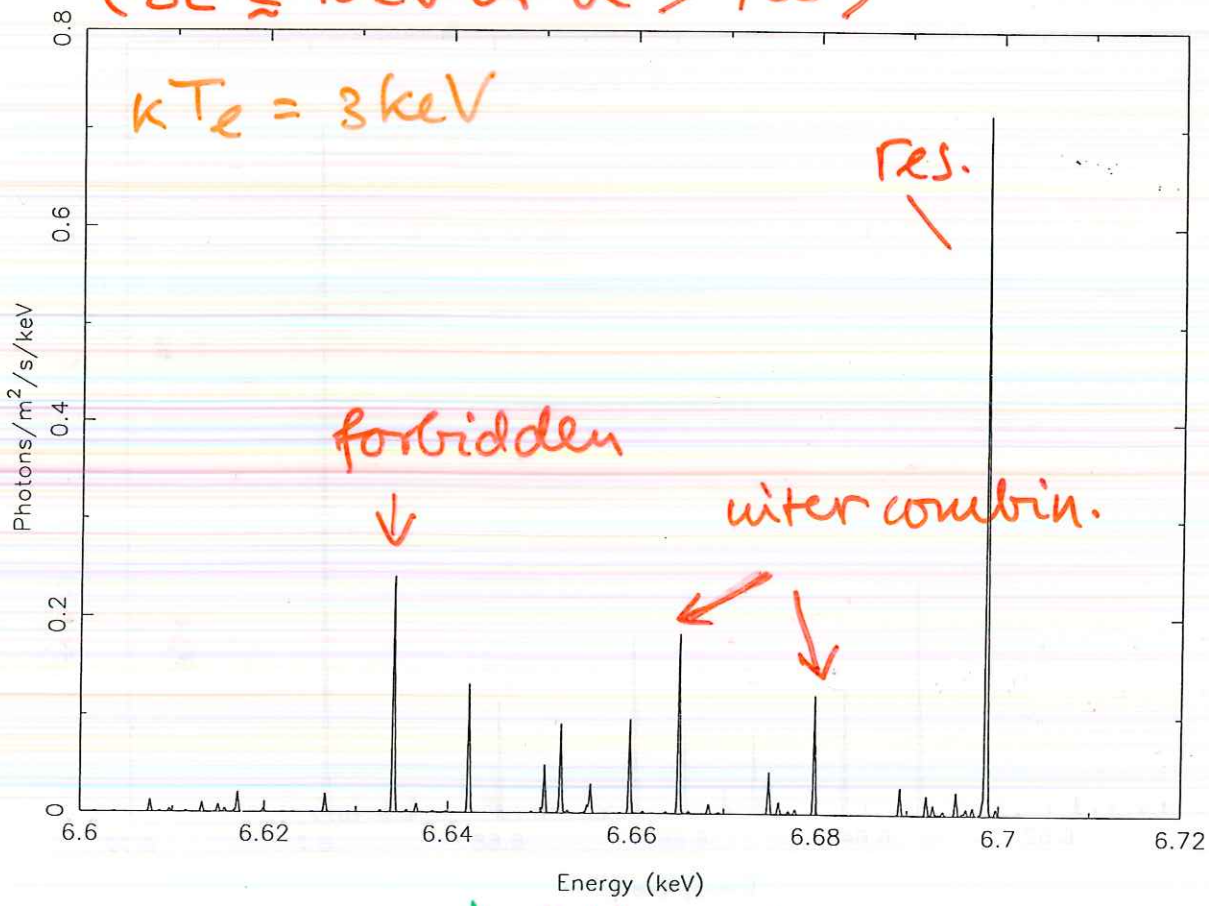

lower charge states (mostly Li-like)

Try this with the XRS on Astro-E :

$\Delta E \sim 12$ eV , $\Delta\varphi \sim 1$ arcmin

Abell 2029 : $r_c \approx 1.5$ arcmin

$kT \sim 7$ keV

τ (FeXXV res.) $\gtrsim 0.5$

total line count : ~ 600 in 100 ksec

$z = 0.0767$

but : non-isothermal (cooling flow); will have to solve for DT as well.

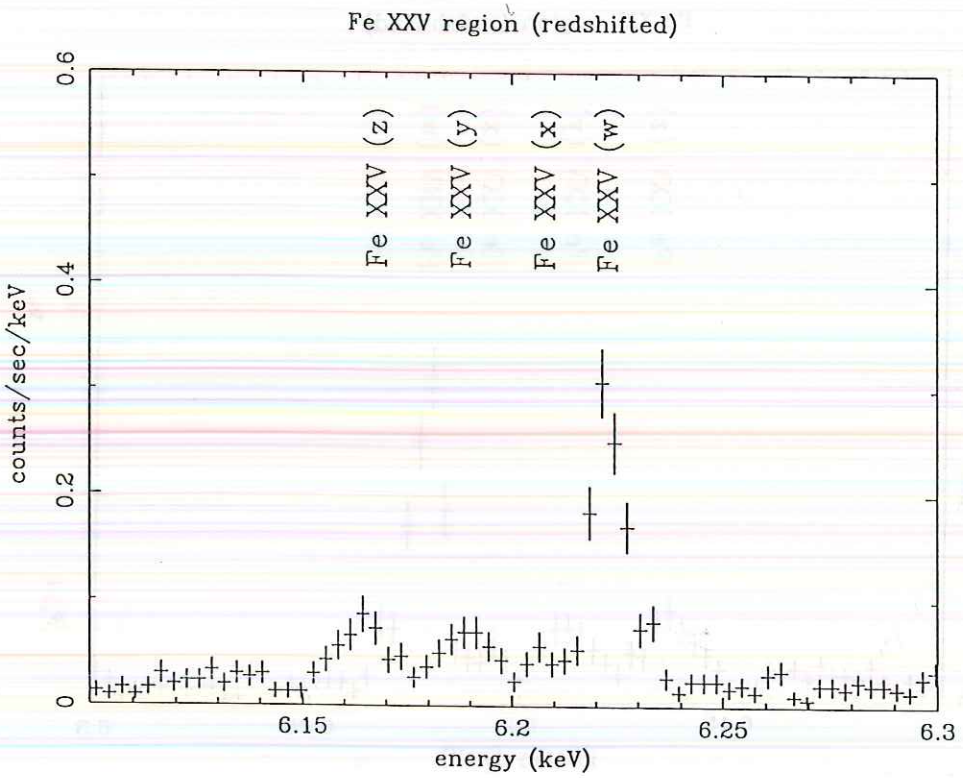

A topic in the Physics of X-ray Spectroscopic Instrumentation, & an Aside on the history of Quantum Mechanics

Diffraction pattern of a Periodic Structure:

(→ efficiency & angular response of grating- and crystal spectrometers)

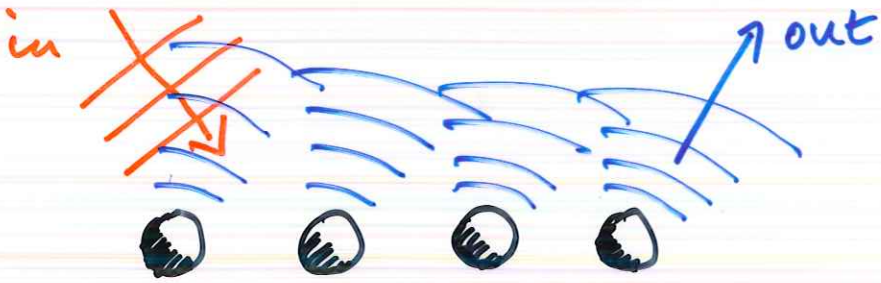

sum the complex phase over all atoms / grating periods:

$$I \propto \left| \sum_n e^{i\vec{k}\cdot\vec{r}_n} \right|^2$$

As old as Friedrich / Knipping / Laue 1912

Debye's objection: thermal vibrations of the ions will destroy the diffraction pattern!

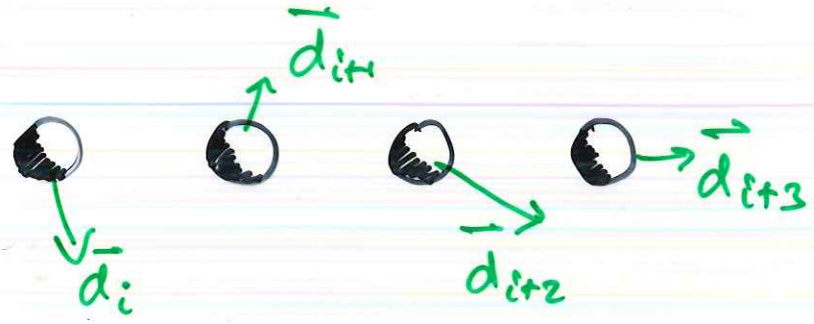

$$\left| \sum_n e^{i\vec{k}\cdot\vec{r}_n} \right|^2 \rightarrow \left| \sum_n e^{i\vec{k}\cdot(\vec{r}_n + \vec{d}_n)} \right|^2 =$$

$$= \sum_n \sum_m e^{i\vec{k}\cdot(\vec{r}_n - \vec{r}_m)} \cdot e^{i\vec{k}\cdot(\vec{d}_n - \vec{d}_m)} \Rightarrow$$

$$\Rightarrow \langle I \rangle = I_0 \cdot \left\langle e^{i\vec{k}\cdot(\vec{d}_n - \vec{d}_m)} \right\rangle$$

$\vec{k}\cdot\vec{d}_n \ll 1$: expand:

$$\left\langle e^{i\vec{k}\cdot(\vec{d}_n - \vec{d}_m)} \right\rangle = 1 + \left\langle i\vec{k}\cdot(\vec{d}_n - \vec{d}_m) \right\rangle -$$

$$- \frac{1}{2} \left\langle (\vec{k}\cdot\vec{d}_n)^2 + (\vec{k}\cdot\vec{d}_m)^2 - 2(\vec{k}\cdot\vec{d}_n)(\vec{k}\cdot\vec{d}_m) \right\rangle +$$

$$+ \ldots = \quad \left(\left\langle (\vec{k}\cdot\vec{d}_n)^2 \right\rangle \equiv \tfrac{1}{3} k^2 \sigma^2 \right)$$

$$\simeq 1 - \tfrac{1}{3} k^2 \sigma^2$$

More generally, for Gaussian $|\vec{d}_n|$:

$$\langle I \rangle = I_0 \cdot e^{-\frac{1}{3} k^2 \sigma^2}$$

↖ Debye-Waller factor

- $\langle I \rangle = e^{-\frac{1}{3}k^2\sigma^2} I_0$

  $\Rightarrow$ fraction $1 - e^{-\frac{1}{3}k^2\sigma^2}$ scattered in between diffraction peaks!

- at room temperature: $k^2\sigma^2 \ll 1$

  ($K \sim \frac{1}{\text{lattice spacing}}$; $\sigma \ll$ lattice spacing)

  $\Rightarrow$ sharp diffraction peaks, faint scattering background, or:

  $\Rightarrow$ Nobel Prize von Laue (1914)
  Debye-Waller factor, Debye

Al K AXAF LETG calibration spectrum

image

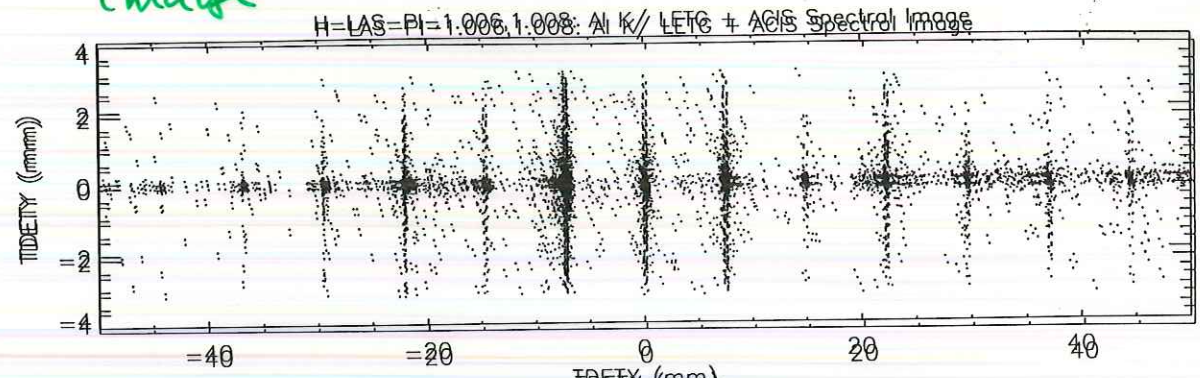

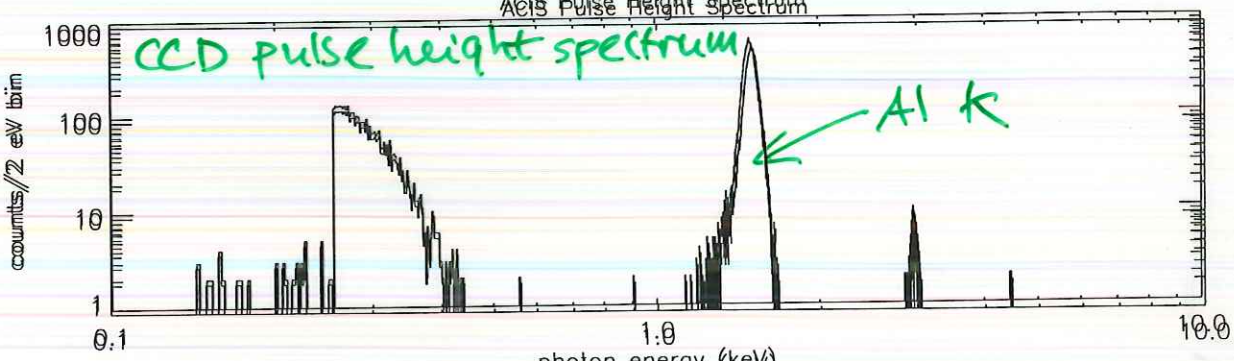

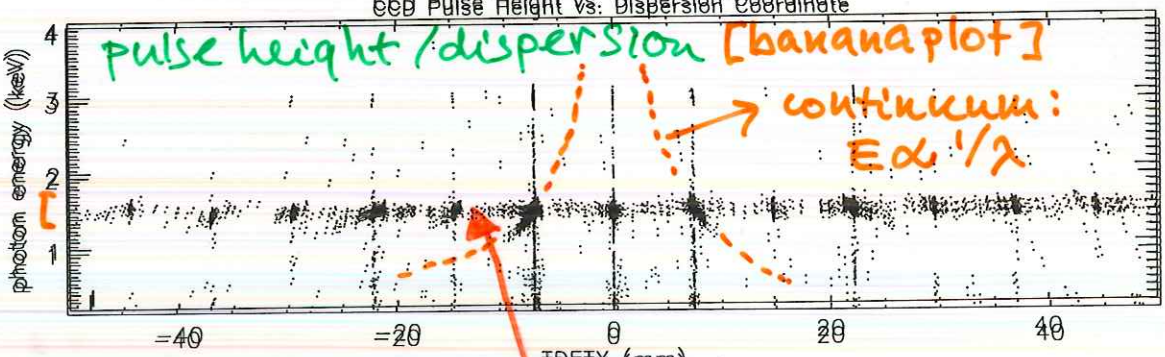

all events same energy →

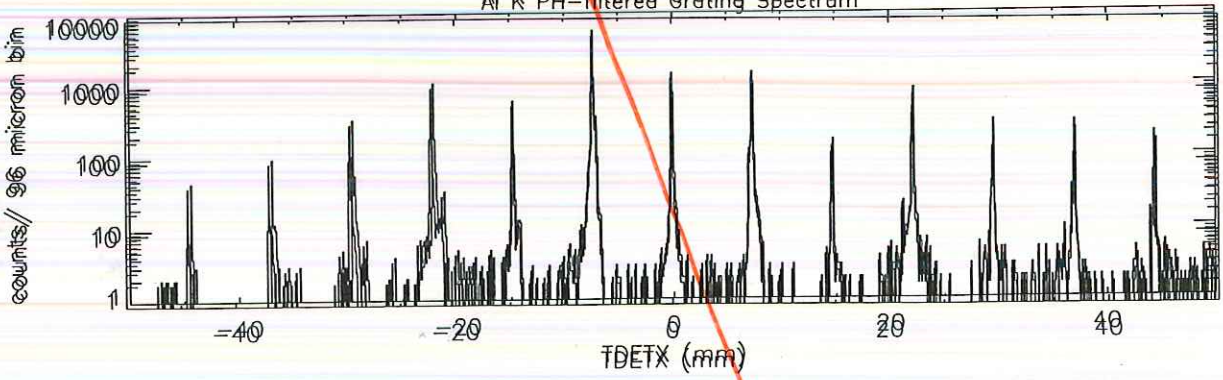

scattered light!

- Scattering by random fluctuations in d !
- σ/d ~ 1% on scales of few grating periods
- amplitude scales as expected w/ wavelength

Debye's Revenge

- Improved calculation for the scattering (i.e. evaluation of $\langle e^{i\vec{k}\cdot(\vec{d}_n - \vec{d}_m)} \rangle$):
- completely analogous to calculation of specific heat of a lattice :
  1) treat ions as coupled oscillators, rewrite eqs of motion in canonical coordinates P_s, Q_s of normal modes $\underline{s}$
  2) Quantize P_s, Q_s according to Bohr-Sommerfeld $\iint_{\text{orbits}} dP_s dQ_s = nh$

  or should we use $\iint dP_s dQ_s = (n+\frac{1}{2})h$??
- SPECIFIC HEAT DOESN'T CARE,

  ($\frac{d}{dT}$ [zero point energy] $= 0$)

  BUT THE SCATTERING DOES !!
- Reduce T to low values: either see, or do not see, residual scattering by zero-point fluctuations !! (this is 1914)

Is this measurable? YES!

$\langle e^{i\vec{k}\cdot(\vec{d}_n-\vec{d}_m)} \rangle \approx e^{-M}$; at low temperatures:

$$M \cong \frac{\hbar^2 x^2}{mk\Theta}(1-\cos\vartheta)\left\{\frac{1}{4}+\frac{\pi^2}{6}\frac{T^2}{\Theta^2}\right\}$$

($x = 2\pi/\lambda$, m: ion mass, Θ: Debye temperature)

due to zero-point motion!

clearly visible for $T \lesssim \Theta$!

DEBYE-WALLER FACTOR, e^{-M}

Interferenz von Röntgenstrahlen und Wärmebewegung. 89

bis zur oberen Horizontale in der Höhe 1 ist proportional der gleichzeitig vorhandenen, zu derselben Wellenlänge gehörigen zerstreuten Intensität, soweit die Veränderlichkeit ihre Ursache in der Wärmebewegung findet.[1])

NO ZPF

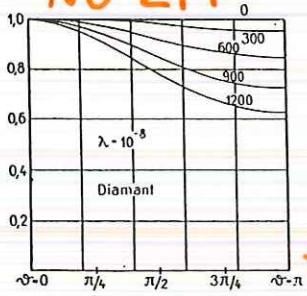

Fig. 4a.

w/ ZPF

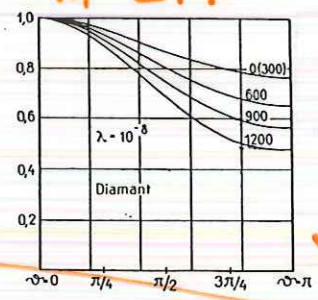

Fig. 4b.

→ DIFFRACTION ANGLE

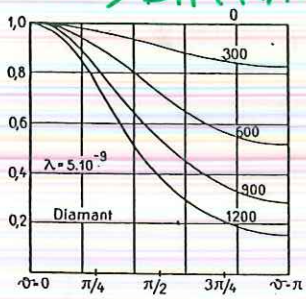

Fig. 5a.

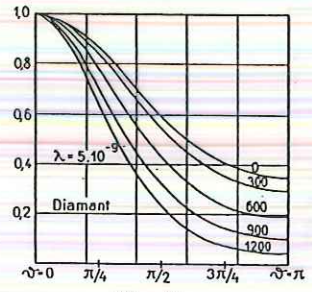

Fig. 5b.

Vor allem zeigen die Figuren den großen Einfluß einer Nullpunktsenergie vorausgesetzt, daß bei genügend kleiner Wellenlänge beobachtet wird. Während nämlich in den Figuren mit dem Index a die Kurve schließlich für $T = 0$ mit der Horizontalen in der Höhe 1 zusammenfällt, ist das bei Anwesenheit einer Nullpunktsenergie nicht der Fall. Wie die Figuren b zeigen ist die Grenzkurve für $T = 0$ erheblich von den ebengenannten horizontalen verschieden, besonders bei der Wellenlänge $3{,}5 \cdot 10^{-9}$. Bei noch kleinerer Wellenlänge würde der Unterschied noch viel größer werden.

1) Für die Reduktion auf die wirklich beobachtbare und im Experiment aufhebende Intensität vgl. man den zweiten Zusatz am Schluß.

$\lambda = 1$ Å x-rays diamond; $\Theta \simeq 1800$ C

← effect increases dramatically with decreasing λ

P. Debye, 1914, Ann. der Physik, 43, 49